



A New Structural Form in the SAM/Metal-Dependent O-Methyltransferase Family: MycE from the Mycinamicin Biosynthetic Pathway

David L. Akey¹, Shengying Li¹, Jamie R. Konwerski¹,
Laura A. Confer^{1,2}, Steffen M. Bernard^{1,3}, Yojiro Anzai⁴,
Fumio Kato⁴, David H. Sherman^{1,5} and Janet L. Smith^{1,2*}

¹Life Sciences Institute, University of Michigan, Ann Arbor, MI 48109, USA

²Department of Biological Chemistry, University of Michigan, Ann Arbor, MI 48109, USA

³Chemical Biology Doctoral Program, University of Michigan, Ann Arbor, MI 48109, USA

⁴Faculty of Pharmaceutical Sciences, Toho University 2-2-1 Miyama, Funabashi, Chiba 274-8510, Japan

⁵Departments of Medicinal Chemistry, Chemistry, Microbiology and Immunology, University of Michigan, Ann Arbor, MI 48109, USA

Received 8 July 2011;
received in revised form
16 August 2011;
accepted 16 August 2011
Available online
23 August 2011

Edited by M. Guss

Keywords:

metal-dependent
methyltransfer;
antibiotic biosynthesis;
macrolide antibiotic;
S-adenosylmethionine-
dependent methyltransfer;
methyltransferase

O-linked methylation of sugar substituents is a common modification in the biosynthesis of many natural products and is catalyzed by multiple families of S-adenosyl-L-methionine (SAM or AdoMet)-dependent methyltransferases (MTs). Mycinamicins, potent antibiotics from *Micromonospora griseorubida*, can be methylated at two positions on a 6-deoxyallose substituent. The first methylation is catalyzed by MycE, a SAM- and metal-dependent MT. Crystal structures were determined for MycE bound to the product S-adenosyl-L-homocysteine (AdoHcy) and magnesium, both with and without the natural substrate mycinamicin VI. This represents the first structure of a natural product sugar MT in complex with its natural substrate. MycE is a tetramer of a two-domain polypeptide, comprising a C-terminal catalytic MT domain and an N-terminal auxiliary domain, which is important for quaternary assembly and for substrate binding. The symmetric MycE tetramer has a novel MT organization in which each of the four active sites is formed at the junction of three monomers within the tetramer. The active-site structure supports a mechanism in which a conserved histidine acts as a general base, and the metal ion helps to position the methyl acceptor and to stabilize a hydroxylate intermediate. A conserved tyrosine is suggested to support activity through interactions with the transferred methyl group from the SAM methyl donor. The structure of the free enzyme reveals a dramatic order–disorder transition in the active site relative to the S-adenosyl-L-homocysteine complexes, suggesting a mechanism for product/substrate exchange through concerted movement of five loops and the polypeptide C-terminus.

© 2011 Elsevier Ltd. All rights reserved.

*Corresponding author. Life Sciences Institute, University of Michigan, Ann Arbor, MI 48109, USA. E-mail address: JanetSmith@umich.edu.

Abbreviations used: SAM, S-adenosyl-L-methionine; SAH, S-adenosyl-L-homocysteine; MT, methyltransferase; OMT, O-methyltransferase; AD, auxiliary domain; SCP-2, sterol carrier protein 2; PDB, Protein Data Bank; SeMet, selenomethionyl; M-VI, mycinamicin VI.

Introduction

Macrolide antibiotics and other natural products are frequently modified with deoxy sugars, many of which are methylated.¹ Differences in hydroxyl methylation can affect solubility, pharmacological properties, and stability of the natural products.² Methylation also can protect hydroxyl groups from undesired modification,² and control of methylation can provide flexibility in synthetic schemes when natural products are used as starting materials for further chemical reactions. The presence or absence of *O*-methyl groups can influence protection/deprotection schemes when targeting specific functional groups for modification. As with all steps involved in natural product assembly, a thorough understanding of the mechanisms and specificity regarding methylation will facilitate efforts to engineer and modify existing natural product biosynthetic pathways with an eye toward optimizing pharmacological properties or using natural products as a starting point for further synthetic modifications.

Mycinamicins are potent antibiotics produced by the actinomycete *Micromonospora griseorubida*, which have activity against Gram-positive bacteria including a number of antibiotic-resistant human pathogens.³ Mycinamicins are composed of a 16-membered macrolactone ring with *O*-linked sugars at the C-5 and C-21 positions (Scheme 1). Mature mycinamicin products contain the 2'',3''-*O*-dimethylated sugar mycinose at the C-21 position and the N, N-dimethylated sugar desosamine at the C-5 position. The macrolactone intermediate protomycinolide IV is assembled by the polyketide synthase pathway encoded by genes *mycAI*–*mycAV*.^{4,5} MycB is proposed to catalyze the addition of desosamine at the C-5 hydroxyl, forming mycinamicin VIII.⁴ Subsequently, MycCI and MycCII catalyze the addition of the C-21 hydroxyl group,⁶ which is the target for 6-deoxyallose addition by MycD, forming mycinamicin VI (M-VI).⁴ The mycinose sugar is the product of methylation of 6-deoxyallose at the 2''-OH by MycE and at the 3''-OH by MycF (Scheme 1).^{7,8} The *S*-adenosyl-L-methionine (SAM)- and metal-dependent methyltransferases (MTs) MycE and MycF are confirmed to react in sequence as MycE cannot methylate mycinamicin III (M-III) and MycF is unreactive toward the 6-deoxyallose sugar on mycinamicin VI.^{7,8}

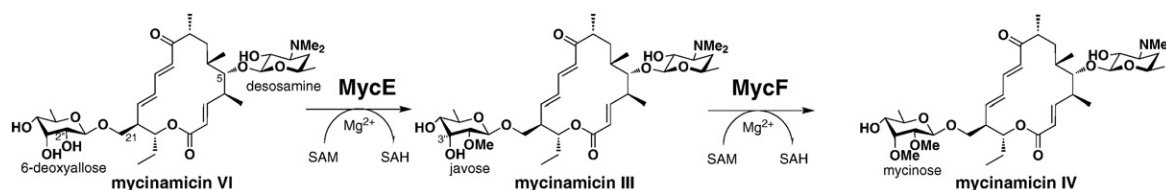
Here, we present crystal structures of MycE that depict the free enzyme, a binary complex with the product *S*-adenosyl-L-homocysteine (SAH), and a ternary complex with SAH and the substrate mycinamicin VI. MycE is a novel tetramer in which three subunits contribute to the active site. An N-terminal auxiliary domain (AD) and a C-terminal α -helix extend away from the MT catalytic domain and contact catalytic domains of neighboring subunits in the tetramer. The AD creates a substrate-binding pocket to one neighboring subunit, and the C-terminal helix caps the active site of another neighboring subunit.

Results

Multi-domain structure

The MycE MT monomer has a two-domain structure (Fig. 1a). The larger C-terminal domain (residues 161–399) is the catalytic MT domain with a typical MT fold.^{9,10} This domain comprises an α/β sandwich with a seven-stranded β -sheet core sandwiched by three α -helices on the front face and two on the back (Fig. 1a and b). The central sheet is parallel with the exception of strand MT β 7 inserted between MT β 5 and β 6. A short 3_{10} -helical segment between MT β 2 and β 3 substitutes for what is typically an α -helix in the MT fold. The C-terminal and N-terminal α -helices (MT α 1 and α 7) and two 3_{10} -helical segments (between MT β 5 and α 6 and between MT α 6 and β 7) are additional elements not found in the minimal MT fold. The closest structural homolog to the MT domain belongs to the catechol *O*-methyltransferase (OMT) family (2.9-Å RMSD, 18% sequence identity; 1VID), whose members are also metal- and SAM-dependent MTs.^{11,12} C-terminal helix MT α 7 (residues 387–395) extends from the subunit, is a critical element in the holomeric assembly of MycE, and may play a role in substrate exchange (see below). The extended loop (residues 371–386) connecting MT α 7 to the body of the MT domain lies at the interface of three monomers of the tetramer, is well ordered in all monomers, and has minimal deviation between monomers (maximum pairwise RMSD of 0.13 Å over all atoms).

The 160 N-terminal residues form an auxiliary domain (AD) that is without precedent among MTs.



Scheme 1. MT reactions in mycinamicin biosynthesis catalyzed by MycE and MycF.

The AD has an α/β structure composed of a four-stranded, mixed β -sheet with a five-helix bundle arranged on one face. A Dali search¹³ identified the closest structural matches in the sterol carrier protein 2 (SCP-2) family.^{14,15} The closest structural homolog among the SCP-2 domains¹⁴ [Protein Data Bank (PDB) ID 2QZT] has just 11% sequence identity and 2.9-Å RMSD with the MycE AD. SCP-2 domains, which are involved in fatty acid transport, typically have a binding site for fatty acids buried within the helix bundle. The AD of MycE has no similar binding site; rather, it mediates the quaternary structure.

Other members of the MycE family likely share the same domain organization. A number of MycE homologues were identified using a BLAST search of the nonredundant protein sequence database.¹⁶ The 26 sequences with greatest identity to the MycE MT core also include an N-terminal region homologous to the MycE AD. All annotated sequences from the search are sugar OMTs in natural product biosynthetic pathways. The MT domains are highly conserved with a pairwise sequence identity of 53% and a minimum of 40% (Fig. S1). In contrast, the AD, which contains no catalytic residues, is less conserved with an average pairwise sequence identity of 25% and a minimum of 10% (Fig. S1).

Tetramer assembly

MycE forms a tetramer with 222 molecular symmetry in which every subunit contacts every other subunit (Fig. 2), consistent with its behavior in solution (see Methods). The primary interface (average 2880-Å² buried surface per monomer) is a domain swap within the MT domains in which the C-terminal helix, MT α 7, caps the adjacent monomer. This interface includes reciprocal interactions between strands MT β 6 from both monomers, forming an extended 14-stranded β -sheet for the combined MT domains. The extended β -sheet across a subunit interface is also seen in the rebeccamycin 4'-OMT RebM (PDB ID 3BUS)¹⁷ and the sarcosine dimethylglycine MT (PDB ID 2O57), which are dimeric enzymes. However, these structures lack the extended linker and terminal MT α 7 helix, which make significant contributions to the MycE interface.

The two other MycE subunit interfaces (average 1970-Å² and 1540-Å² buried surface per monomer) are formed through reciprocal interactions between the MT domain and AD (Fig. 2). The quaternary arrangement has functional implications, as three subunits contribute to each of the four substrate-binding pockets (see below).

Active-site architecture

The SAM binding site is located within the loops at the C-terminal edge of the central MT β -sheet

(underlined residues in Fig. 1c), as usual for MTs. In addition to clear density for SAH, we observed coordination of a metal ion by residues Asp275, Glu303, and Asp304 (Fig. 3a, dotted residues in Fig. 1c) in accord with the metal dependence of activity.⁷ These residues are strictly conserved among the MycE homologs, implying that all homologs are metal dependent (Fig. S1). Asp275 and Glu303 are positioned by H-bonds with the invariant Lys175. The coordination of a metal ion by two adjacent residues immediately C-terminal of MT β 5 and a third residue at the C-terminus of MT β 4 is also observed in the MycF/TyIF and catechol OMT families.^{12,18} Interactions with SAM are provided by H-bonds of the ribose 2' and 3' hydroxyl groups with the carboxylate of the conserved Asp234 and of the adenine N6 with Asp252 (Fig. 3b). The SAM amino acid moiety is hydrogen bonded with Thr173 through the carboxyl group and with Glu202, Ser217, and Asp275 through the amino group. As with the metal ligands, the residues that contact SAM are highly conserved.

In addition to the product SAH, we introduced the substrate mycinamicin VI into crystals through soaking. The density for the two sugar groups and for much of the macrolactone ring was readily apparent in the difference electron density maps (Fig. S2). The macrolactone ring binds in a predominantly hydrophobic pocket, which is formed at the interface of the catalytic domain from one monomer (Fig. 4, blue), the AD from a second monomer (Fig. 4, green), and the C-terminal helix MT α 7 from a third monomer (Fig. 4, yellow). Upon macrolide binding, the N-terminal segment of helix AD α 5 from the second monomer is shifted toward from active site (Fig. 5, green). Rearrangement of the macrolide binding pocket through helix AD α 5 movement is similar to, although much less dramatic than, the rearrangement seen upon binding of substrates in the caffeic acid OMT involved in lignin biosynthesis.¹⁹

The 6-deoxyallose sugar docks in the chair conformation with the 2''- and 3''-OH groups coordinating the active-site magnesium (Fig. 4 and Fig. S2). In concert with two aspartate carboxylates (Asp275 and Asp304) and two water molecules, these interactions complete the octahedral coordination of the magnesium ion. Interestingly, the magnesium ion moves ~1 Å upon binding of mycinamicin VI, resulting in the loss of the Glu303 ligand, which is replaced by a water molecule (Fig. S2). The coordination of metal by three protein ligands and by the methyl acceptor hydroxyl group and an adjacent hydroxyl is similar in MycE, in metal-dependent catechol MTs,^{11,12} and in RNA MTs.²⁰ However, in the catechol OMT family, the metal remains coordinated by all three residues upon binding of the methyl acceptor mimics.¹²

Generally, SAM-dependent OMTs employ acid-base chemistry to deprotonate the OH methyl

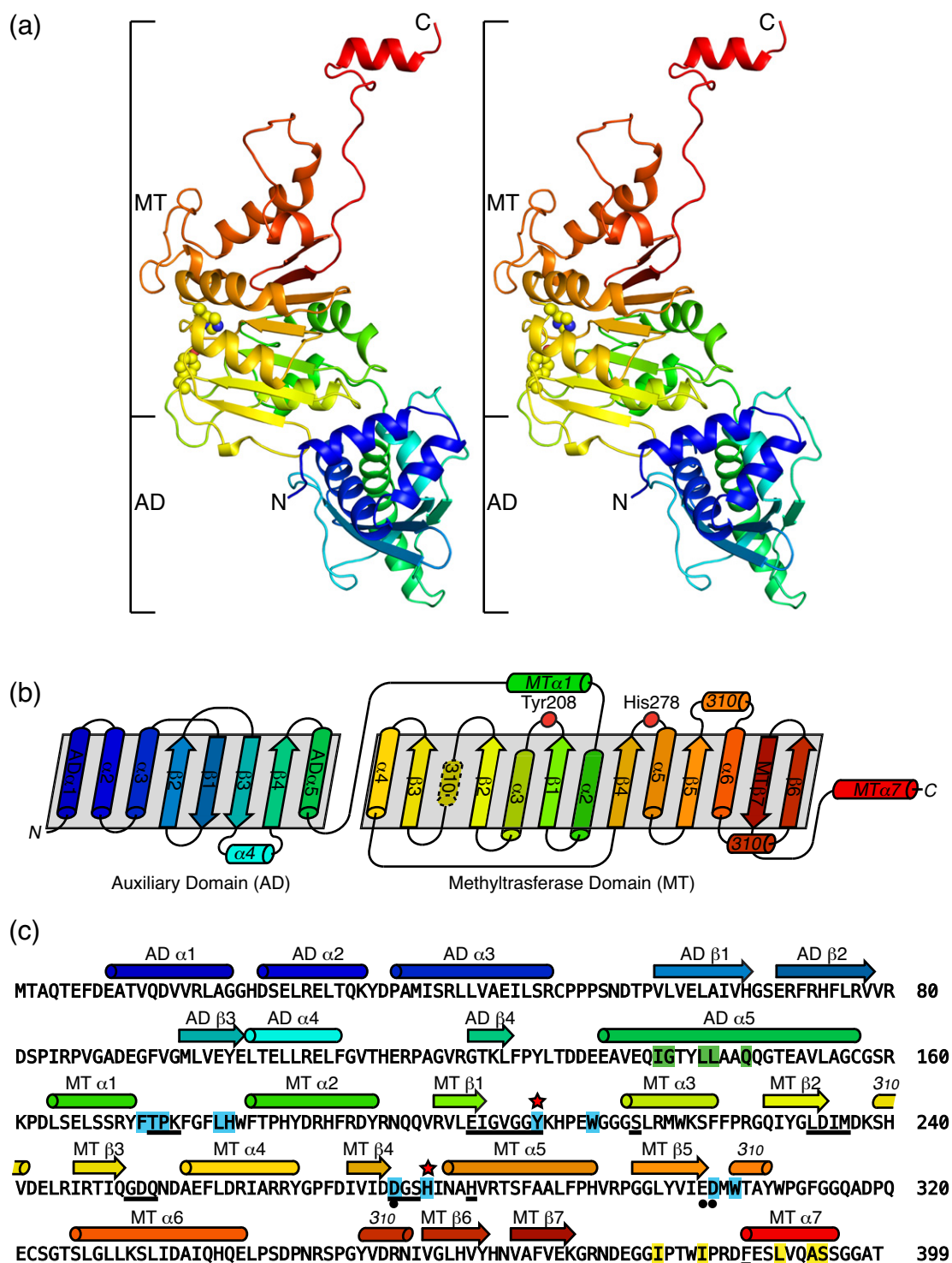


Fig. 1. MycE structure. (a) Stereo diagram of MycE monomer. The MT and AD are indicated on the left. The polypeptide is colored as a rainbow from the blue N-terminus to the red C-terminus. Active-site Tyr208 and His278 are shown as spheres. (b) MycE topology. Coloring is as in (a). Active-site residues are labeled. (c) MycE sequence and secondary structure assignment. Active-site Tyr208 and His278 are indicated with stars. Underlined residues form the SAM binding site. Highlighted residues form the inter-subunit mycinamicin VI binding pocket with colors indicating the subunit of origin for the active site in the upper right of Fig. 2a (AD, green; MT domain, blue; and MT $\alpha 7$, yellow, consistent with Figs. 2, 4, and 5). Residues with black dots coordinate the active-site magnesium ion.

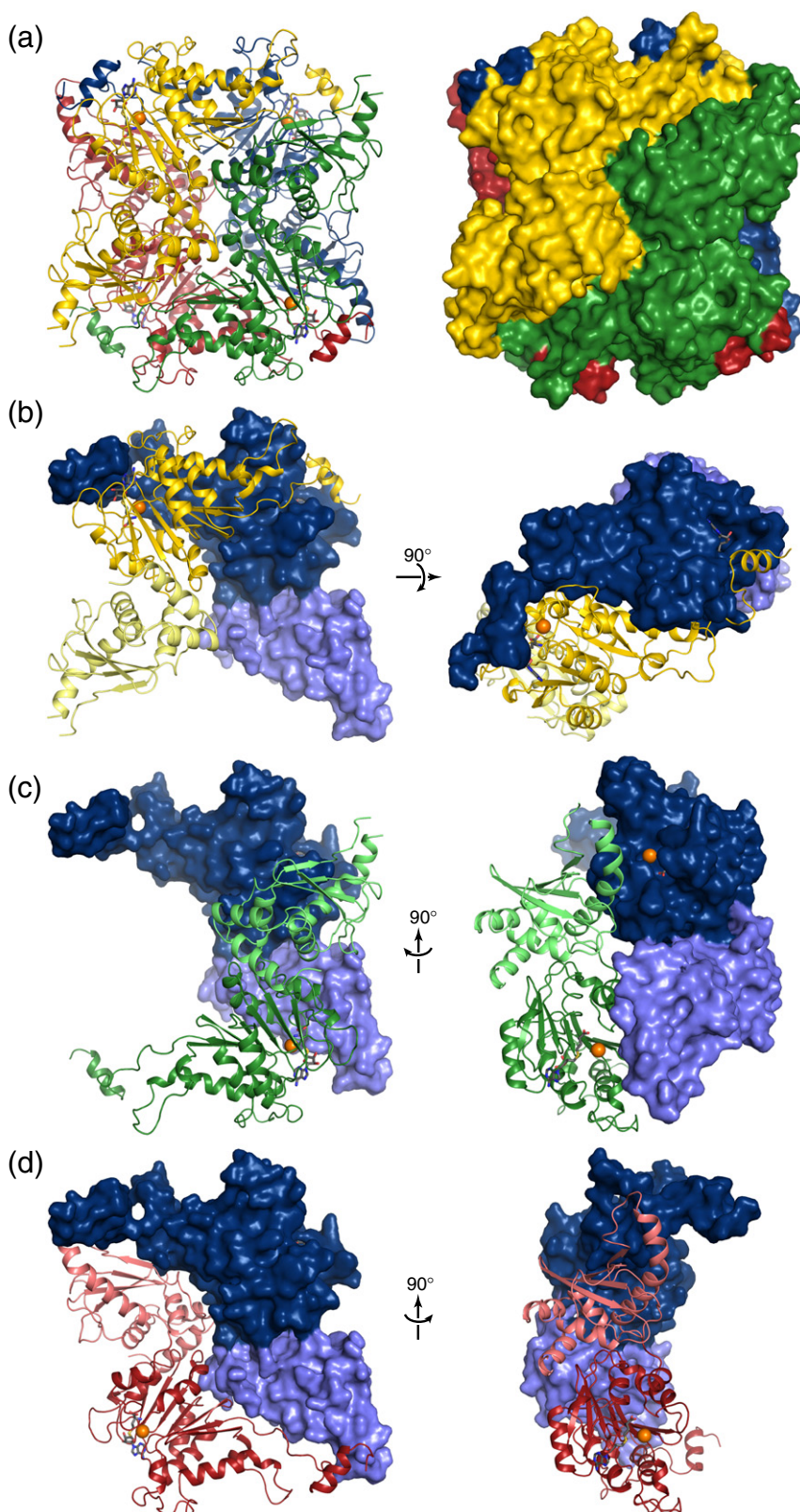


Fig. 2. MycE quaternary structure. (a) MycE tetramer in cartoon (left) and surface (right) representations. SAH (gray sticks) and magnesium ions (orange spheres) are shown at each of the four active sites. The yellow monomer is rotated $\sim 45^\circ$ clockwise with respect to the monomer in Fig. 1a. (b) Primary subunit interface (blue and yellow subunits). Note the domain swap of MT domains (darker shades) in which the C-terminal helix MT $\alpha 7$ contacts the active site of the partner subunit. (c) Secondary interfaces of blue and green subunits. Reciprocal interactions between MT domains (dark shades) and ADs (light shades) bring the AD $\alpha 5$ helix adjacent to the active site of the partner subunit. (d) Secondary interfaces of blue and red subunits. Reciprocal interactions between MT domains (dark shades) and ADs (light shades) result in no contacts with the active-site region of the partner subunit.

acceptor prior to attack of the SAM methyl group by the resulting hydroxylate. In the MycE–mycinamicin VI complex, the methyl acceptor 2''-OH is

positioned between the methyl group of SAM and the invariant residue His278, which is optimally positioned for proton abstraction. Residues of

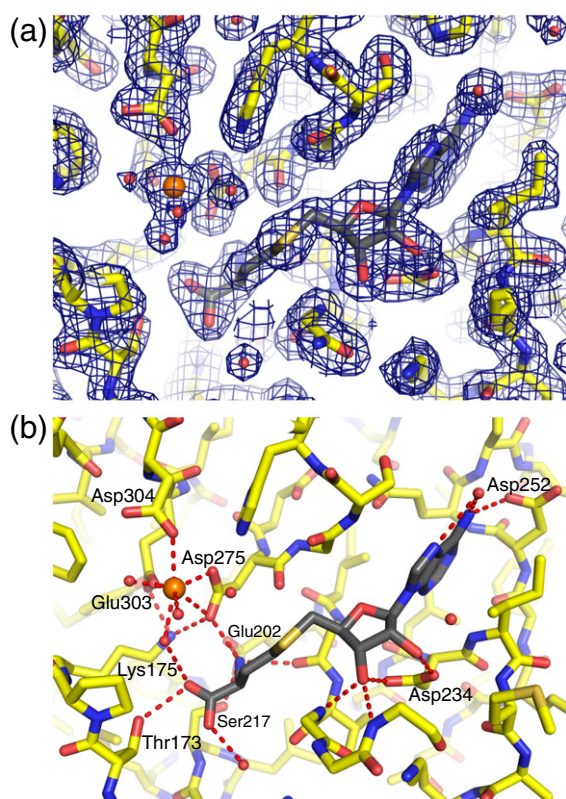


Fig. 3. MycE active site. (a) Active-site electron density map ($2mF_o - F_c$, 1.9 Å, contoured at 1.2 σ) showing SAH (gray C), protein (yellow C), Mg (orange sphere), and waters (red sphere). (b) SAH and magnesium binding. H-bonds with conserved binding residues are indicated as broken lines.

different type have been proposed to serve as the general base in different MT families: In NovP, a representative of the MycF/TylF family, the base is a conserved aspartate;¹⁸ in the catechol OMT family, a lysine;¹² and in the RebM family, a histidine.¹⁷ Using the position of SAH to model the methyl donor SAM, we assembled a full picture of the substrate complex and devised a complete structure-based reaction mechanism (Scheme 2). Specifically, His278 acts as a general base, removing the proton from the 2''-OH leaving a hydroxylate anion, which is stabilized by interactions with the magnesium cation. Subsequently, the 2'' hydroxylate abstracts the methyl group from SAM to complete the reaction. Tyr208 is adjacent to SAH and highly conserved, but its closest contact to one of the substrates is with the methyl group of the SAM donor. Interestingly, in the SET-domain histone MTs, CH-O hydrogen bonding, including interactions with a conserved tyrosine, was proposed to facilitate the transfer of a methyl from SAM to the acceptor substrate.²¹ Thus, Tyr208, which interacts in a fashion almost identical with

that of the SAM methyl group, may have a similar role in MycE.

Comparisons with other metal-dependent MTs

Mechanistically, MycE is comparable to two other families of small-molecule metal-dependent OMTs of known structure, including catechol OMT^{11,12} and the MycF/TylF MTs, of which the novobiocin MT NovP is the prototype structure.¹⁸ While these small-molecule metal-dependent MTs are no more closely related at the sequence level than are other MT families, the three side chains that coordinate the metal are at topologically equivalent positions, strongly suggesting that they have a common metal-dependent MT ancestor. Another common feature of the metal-dependent OMTs is the metal ion coordination of adjacent substrate hydroxyl groups in the methyl acceptor. The proposed substrates for members of the MycE/TylE family and also the MycF/TylF family (NovP)^{22–29} all contain adjacent hydroxyl groups at the site of methylation. Interestingly, the identity of the catalytic base differs in the three families, with a histidine serving as the base in the MycE/TylE family; an aspartate, in the MycF/TylF family,¹⁸ and a lysine, in the catechol OMT family.¹² Despite differences in base identity, the basic residues are in identical topological locations in all three MT families (Fig. S3). In certain cases, for example, in the spinosad and butenyl-spinosyn biosynthetic pathways,^{23,27} methylation occurs adjacent to a hydroxyl that was previously methylated, suggesting that the metal ion may coordinate an O-methyl-hydroxyl pair. It remains to be seen how much flexibility exists with regard to modifications of the hydroxyl group adjacent to the methyl acceptor.

Activity of MycE with active-site substitutions

To test the proposed mechanism, we made single-residue substitutions of His278 (Ala, Gln, and Lys) and Tyr208 (Phe) (Table 1). As the residue corresponding to the conserved His278 is strictly conserved as a lysine in the catechol OMT family,¹² the H278K substitution tested whether lysine will support activity in the MycE family. However, none of the histidine substitutions had detectable activity (Table 1 and Fig. S4). The lack of activity for H278A and H278Q confirms that a general base is required and that a H-bond donor/acceptor pair incorporating the 2''-OH is not sufficient to support methyl transfer. H278K lacks activity, suggesting that other differences between the active sites of the MycE and catechol OMT families are required for lysine to serve as an effective base. Y208F MycE has 3- to 4-fold lower activity than wild-type MycE, consistent with a weak stabilizing CH-O interaction of the Tyr208 hydroxyl and the SAM methyl. The

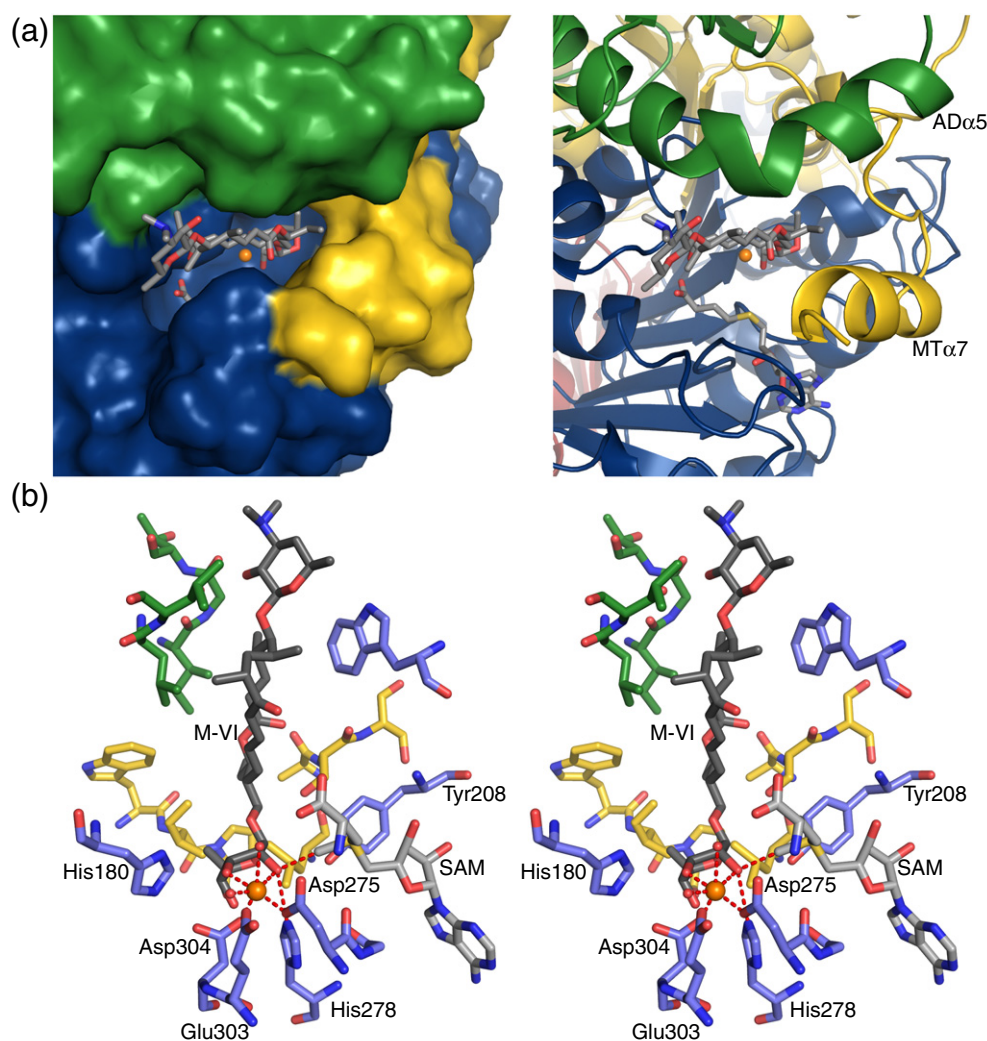


Fig. 4. Substrate binding. (a) Binding pocket for mycinamicin VI (M-VI) (sticks with gray C) at the junction of three monomers (blue, green, and yellow surfaces). The catalytic site is located on the blue monomer. The region of the green monomer is the AD. The coloring is as in Fig. 1b. The residues that form the mycinamicin VI binding site are highlighted in Fig. 1c (blue, green, and yellow). The surface is removed in the right-hand image. (b) Stereo diagram of mycinamicin VI binding site. C atoms are colored as in (a). Mycinamicin VI is shown with dark-gray C. SAM (light-gray C) is modeled based on SAH binding.

effect of the Y208F substitution is not as dramatic as for the SET methyltransferases, for which the corresponding tyrosine-to-phenylalanine substitution completely ablates activity.²¹ In contrast to the histidine and tyrosine substitutions, the benign Ile279-to-valine variant has activity comparable to that of wild-type MycE.

Active-site rearrangement

A view of the MycE free enzyme is captured in one of the crystal structures, revealing a remarkable transformation of the active site. In one of the four active sites in form 1 crystals, no SAH is bound, and the active site is disordered including most residues for binding SAM, metal, and mycinamicin as well as

the catalytic residues. A total of 39 residues in active-site loops from the catalytic subunit (Fig. 5, blue) are disordered, including the loops following MT α 1, MT β 1, MT β 4, and MT β 5. Additionally, in an adjacent subunit (Fig. 5, yellow), 29 residues are disordered, including the loop after MT α 6 and the C-terminal helix MT α 7. In contrast, the SAH-bound active sites are well ordered, with SAH deeply buried, suggesting that the observed opening of the active site is required for exchange of SAH for SAM. Once SAM is bound, the docking site for mycinamicin VI is re-formed, and the reaction proceeds. A similar exchange mechanism may occur in other families of SAM- and metal-dependent MTs: In the catechol OMT family, structural rearrangement coincident with the presence or absence of SAM

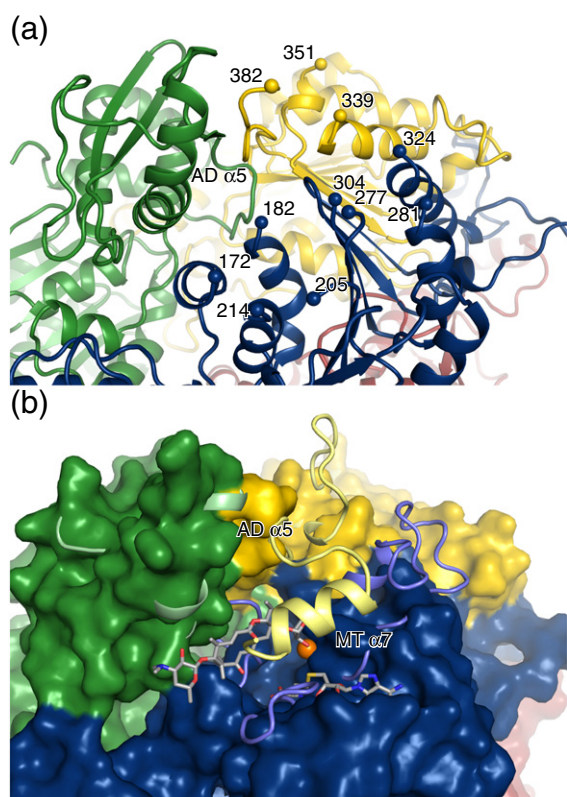
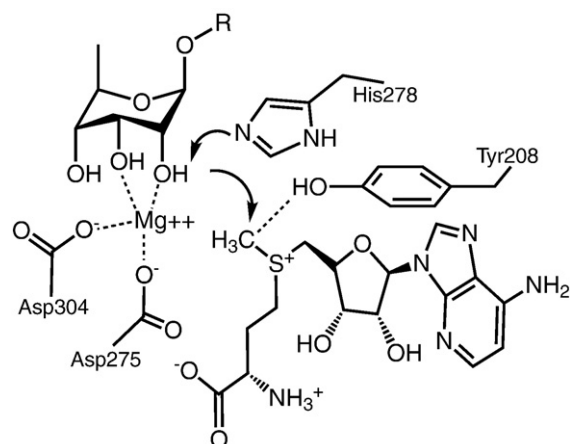


Fig. 5. Order-disorder transition in the active site. (a) Active site in the free enzyme. Coloring is as in Figs. 2 and 4. The blue subunit contains catalytic residues; the yellow subunit contributes the MT $\alpha 7$ helix, and the green subunit, the AD. The residues at the order-disorder boundaries (spheres) are numbered. (b) Superposition of active sites from the free enzyme and the ternary complex with mycinamicin VI and SAH, viewed in the same orientation as in (a). The surface is shown for the disordered, free-enzyme catalytic site [colored as in (a)]. Mycinamicin VI, SAH (sticks with gray C), and Mg^{2+} (orange sphere) are shown in the active site. The ternary complex is rendered as a ribbon to highlight those regions that are ordered by SAM binding (residues 173–181, 206–213, 278–280, and 305–323 of the blue subunit and residues 340–350 and 382–399 of the yellow subunit).

is observed in several loops equivalent to those that undergo order-disorder transition in MycE.³⁰ Additionally, in the structure of NovP, a member of the MycF/TylF family, two helices inserted between $\beta 2$ and $\beta 3$ cap the active site, have elevated temperature factors, and are proposed to move for SAH/SAM exchange.¹⁸ Interestingly, when the MycE and NovP structures are superposed, helix MT $\alpha 7$ from the adjacent MycE subunit aligns with the second of the lid helices in the monomeric NovP, suggesting a similar gating mechanism of the SAM site for SAH/SAM exchange in both systems. Computational analysis is consistent with the structural observations (Fig. S5).



Scheme 2. Proposed mechanism of MycE-catalyzed methyltransfer.

Discussion

The SAM-dependent MTs are a large superfamily whose members have the same folding topology, bind SAM in the same manner, and are thought to have diverged from a common MT ancestor. However, the many branches of the superfamily have highly divergent sequences and cannot be compared in absence of structures. The MycE structure reported here is the prototype for a third family of natural product sugar MTs. The two other families for which structural data are available are the metal-dependent MycF/TylF MTs¹⁸ and the rebeccamycin MT (RebM) family, which is not metal dependent.¹⁷

In accord with the high degree of MT divergence, a number of novel features are observed in the MycE structure. While a number of discrete oligomeric assemblies have been described for members of the MT superfamily, the tetrameric arrangement of MycE has not been observed previously. Use of the AD as both an essential component of tetramer assembly (Fig. 2) and a part of the substrate-binding pocket (Fig. 4) is unique among MTs and is also a novel function for the SCP-2-like fold found in the AD. The fusion of the SCP-2-like AD to the MT N-terminus is critical for conversion from a presumably dimeric MT precursor to the observed tetramer.

Interestingly, the quaternary assembly occurs without any AD-AD interactions (Fig. 2), suggesting that the SCP-2-like AD precursor was monomeric.

Table 1. Measured activity for MycE mutants

MycE variant	% Activity (SD)
Wild type	100 (5.6)
H278A	n.d.
H278Q	n.d.
H278K	n.d.
Y208F	29 (3.4)
I279V	109 (6.1)

Because the SCP-2 proteins are sterol binders, it is tempting to speculate that the precursor of the AD may have been a hydrophobic binding protein that brought a mycinamicin binding capability to the MT precursor. However, the MycE substrate-binding pocket is formed equally by AD and MT domains and does not include elements of the SCP-2 sterol binding site. Another novel feature of MycE and homologs is the domain swap of the C-terminal helix MT $\alpha 7$ across the MT–MT subunit interface, which is otherwise similar to subunit interfaces in dimeric MTs. We speculate that the domain swap may also occur in other dimeric MTs that lack an AD, although this is impossible to predict from sequence data alone.

The ability of natural product biosynthetic enzymes to act on nonnatural substrates is an overarching concern for efforts to introduce chemical diversity into complex natural products such as mycinamicin by chemoenzymatic synthesis.^{31,32} The absence of specific interactions between MycE and the mycinamicin macrolactone ring or the desosamine sugar suggests that the enzyme will tolerate a significant degree of variability in these groups. The primary constraint on substrate diversity would be to maintain the hydrophobic character and the relatively compact, flat shape of the macrolactone ring. Further testing of members of the MycE family with nonnatural substrates may yield insights as to the degree of substrate modifications that can be introduced without impairing methylation. Structures have been determined for substrate complexes of a number of macrolide processing enzymes, including those responsible for cyclization,³³ glycosylation,³⁴ oxidation,^{35–37} and here for methyl transfer. These enzymes typically lack specific contacts with the macrolide ring; rather, they have in common a predominately hydrophobic binding pocket, which may be accessible to a wide range of macrolactone substrates. Indeed, a number of these enzymes have demonstrated flexibility in substrate specificity.^{38–40} Such flexibility should facilitate engineering of novel biosynthetic products in that requirements for specific interactions may be limited to the immediate catalytic environment and not to the overall identity of the macrolactone ring and its auxiliary modifications.

Methods

Protein production and crystallization

The N-terminal His₆-tagged MycE was expressed from pET28b-mycE in *Escherichia coli* strain BL21 (DE3).⁷ The protein was purified by Ni-NTA affinity chromatography followed by gel-filtration chromatography in 150 mM NaCl, 10% glycerol, Tris (pH 7.5), and 2 mM DTT on a Sephadex S200 column from which it eluted as a tetramer (apparent molecular mass, 210 kDa; monomer molecular mass, 45 kDa). Selenomethionyl (SeMet) MycE was produced

using a protocol modified from Guerrero *et al.* in which cells from a 100-mL overnight culture were added to SeMet-supplemented minimal media prior to induction.⁴¹ MycE crystals were grown in the presence of 5 mM SAM or SAH by hanging-drop vapor diffusion, equilibrating a mixture of 2 μ L of protein (\sim 10 mg/mL) with 1 μ L of well solution (20–25% polyethylene glycol 3350, 0.15 M NaCl, and 0.1 M 2-[bis(2-hydroxyethyl)amino]-2-(hydroxymethyl)propane-1,3-diol, pH 6.0–6.5). Two crystal forms grew in similar conditions. Form 1 crystals typically grew in clusters of needles with the occasional blocks (up to 50 μ m \times 50 μ m \times 200 μ m, space group $P2_1$), which diffracted to 2.25 Å. Form 2 crystals, hexagonal plates (space group $C222_1$), which diffracted to 1.9 Å, grew in approximately 1% of the wells. Prior to cooling in liquid nitrogen, crystals were transferred to a cryoprotection solution equivalent to well solution with 25% polyethylene glycol 3350 and 5% glycerol. Mycinamicin VI was soaked into crystals that were grown with the addition of 5% dimethyl sulfoxide in the well solution. Crystals were soaked overnight in a cryoprotection solution with 5% dimethyl sulfoxide and 5 mM mycinamicin VI prior to harvesting.

Structure solution

Data were collected at beamline 23ID-D (National Institute of General Medical Sciences and National Cancer Institutes Collaborative Access Team) at the Advanced Photon Source and processed with HKL2000.⁴² Phaser,⁴³ as implemented in the PHENIX program suite,⁴⁴ was used to solve the structure of MycE in the $P2_1$ crystal form 1 by the single-wavelength anomalous diffraction method. To optimize the anomalous signal, we used combined data from three SeMet MycE crystals to determine the heavy-atom substructure and subsequent phases. The asymmetric unit of the $P2_1$ crystal form contains a tetramer with 399 residues per monomer. Nineteen of the expected 20 Se sites (with 4 in double locations) plus 2 additional sites for selenated SAH were located. RESOLVE^{45,46} was used for solvent flattening, 4-fold averaging, and initial automated building of an 85% complete model. The model was refined against a native data set collected from a single crystal. Coot⁴⁷ was used for model building, and REFMAC5, for refinement. Molecular TLS (translation/libration/screw)^{48,49} modeling of molecular motion was used during refinement with four TLS domains per monomer assigned by the TLSMD server.⁵⁰ A single subunit from the structure in space group $P2_1$ was used as the search model to solve the MycE structure in the $C222_1$ crystal form 2. Six subunits were located in the asymmetric unit, corresponding to an intact tetramer and half of a second tetramer, which is completed by crystallographic symmetry. Regardless of whether MycE crystals were grown in the presence of SAM or SAH, no density for the SAM methyl group was observed; subsequently, SAH is modeled in all structures. One subunit of MycE in the $P2_1$ crystal form contained no SAH. Model geometry was checked using MolProbity.^{51,52} There are no Ramachandran outliers. Data collection and refinement statistics are reported in Table 2. Multiple sequence alignment was done with CLUSTAL^{53,54} and displayed with JALVIEW⁵⁵ (Fig. S1). Alignments were manually modified to eliminate gaps in regions of defined secondary structure. Figures were created using PyMOL.⁵⁶

Mutagenesis

Site-directed mutagenesis was performed using the QuikChange Site-Directed Mutagenesis Kit (Stratagene). The pET-28b-*mycE* expression plasmid⁷ was employed as the PCR template. DNA sequencing at the DNA Sequencing Core of the University of Michigan verified the mutated genes. The plasmids carrying mutant *mycE* genes were used for transforming the overexpression strain *E. coli* BL21 (DE3). The purification of mutant MycE followed the procedure previously developed for the wild-type MycE.⁷ The following primers were used for site-directed mutagenesis (modified codons in italics):

Y208F: 5'-GGTGTCTGGAGGCTTCAAACACCCG-GAG-3',
 5'-CTCCGGGTGTTTGAAGCCTCCGACACC-3';
 H278A: 5'-CGACGACGGTAGCGCCATCAACGCC-CACG-3',
 5'-CGTGGGCGTTGATGGCGCTACCGTCGTCG-3';
 H278K: 5'-CATCGACGACGGTAGCAAGATCAA-CGCCCCACGTGC-3',

5'-GCACGTGGGCGTTGATCTTGCTACCGTCGTC-GATG-3';
 H278Q: 5'-CGACGACGGTAGCCAGATCAACGCC-CACG-3',
 5'-CGTGGGCGTTGATCTGGCTACCGTCGTCG-3';
 and
 I279V: 5'-GACGGTAGCCACGTCAACGCCCCACG-TG-3',
 5'-CACGTGGGCGTTGACGTGGCTACCGTC-3'.

Activity assays

Enzymatic assays followed the procedures previously reported.⁷ Briefly, 2 μ M enzyme, 250 μ M mycinamicin VI, 10 mM MgCl₂, and 500 μ M SAM (Sigma-Aldrich) in 100 μ L of 50 mM Tris buffer, pH 9, were incubated 1 h at 50 °C. Mycinamicin VI was isolated and purified from the fermentation broth of *mycE* disruption mutant *M. griseorubida* TPMA0003.⁸ Reactions were quenched, and the product was extracted by addition of CHCl₃ (2 \times 200 μ L). Organic extracts were dried and redissolved in 120 μ L

Table 2. Crystallographic data and refinement statistics

	Form 1			Form 2
	SeMet	Native	MycE + M-VI	Native
<i>Data</i>				
Space group	<i>P</i> 2 ₁	<i>P</i> 2 ₁	<i>P</i> 2 ₁	<i>C</i> 222 ₁
Cell <i>a</i> , <i>b</i> , <i>c</i> (Å)	73.70, 142.46, 84.04	73.9, 143.41, 84.64	73.11, 142.11, 83.86	144.22, 250.85, 158.32
Cell β (°)	105.9	105.6	105.6	90
<i>d</i> _{min} (Å)	2.60 (2.69–2.60) ^a	2.25 (2.33–2.25)	2.40 (2.49–2.40)	1.90 (1.97–1.90)
I/ σ _I	24.0 (3.2)	13.4 (2.4)	13.2 (2.05)	19.5 (2.7)
<i>R</i> _{symm}	0.182 (0.998)	0.087 (0.614)	0.077 (0.688)	0.121 (0.511)
Redundancy	10.4 (6.8)	3.9 (3.9)	3.4 (3.3)	6.8 (3.8)
Completeness	100 (100)	100 (100)	99.1 (99.3)	96.3 (76.3)
Se sites	26			
SOLVE FOM	0.24			
RESOLVE FOM	0.74			
Wilson <i>B</i> (Å ²)		35.4	47.5	22.8
<i>Refinement</i>				
No. of reflections		76,211	64,796	205,672
<i>R</i> _{work} / <i>R</i> _{free}		0.165/0.210	0.165/0.218	0.144/0.177
RMSD bonds (Å)		0.007	0.008	0.008
RMSD angles (°)		1.029	1.133	1.061
No. of atoms				
Protein		11,926	11,901	19,467
Water		845	522	2780
SAH/Mg		81	81	162
Mycinamicin VI			94	
<i>B</i> -factors (Å ²)				
Protein		41.9	50.8	27.6
Water		40.4	47.1	37.8
SAH/Mg		43.0	52.7	21.3
Mycinamicin VI			64.4	
Ramachandran (%)				
Favored		97.7	96.9	98.3
Allowed		2.3	3.1	1.7
PDB ID		3SSM	3SSN	3SSO

FOM, figure of merit.

^a Numbers in parentheses refer to the outermost shell of data.

methanol. Product formation was quantified by monitoring absorbance at 280 nm during reverse-phase HPLC (C₁₈ column Waters: 3.5 µm, 150 mm) with a 20–100% acetonitrile plus 0.1% formic acid gradient in deionized water supplemented with 0.1% formic acid. Conversion ratios were calculated based on duplicated experiments.

Accession numbers

Atomic coordinates and structures factors have been deposited in the PDB with accession codes 3SSM for MycE crystal form 1, 3SSN for form 1 with mycinamicin VI, and 3SSO for crystal form 2.

Supplementary materials related to this article can be found online at [doi:10.1016/j.jmb.2011.08.040](https://doi.org/10.1016/j.jmb.2011.08.040)

Acknowledgements

This work was supported by National Institutes of Health grant DK042303 to J.L.S. and National Institutes of Health grant GM078553 and the Hans W. Vahlteich Professorship to D.H.S. GM/CA CAT has been funded in whole or in part with Federal funds from the National Cancer Institute (Y1-CO-1020) and the National Institute of General Medical Sciences (Y1-GM-1104). Use of the Advanced Photon Source was supported by the US Department of Energy, Basic Energy Sciences, Office of Science, under contract No. DE-AC02-06CH11357.

References

- Thibodeaux, C. J., Melancon, C. E. & Liu, H. W. (2007). Unusual sugar biosynthesis and natural product glycodiversification. *Nature*, **446**, 1008–1016.
- Zubieta, C., He, X. Z., Dixon, R. A. & Noel, J. P. (2001). Structures of two natural product methyltransferases reveal the basis for substrate specificity in plant O-methyltransferases. *Nat. Struct. Biol.* **8**, 271–279.
- Satoi, I., Muto, N., Hayashi, M., Fujii, T. & Otani, M. (1980). Mycinamicins, new macrolide antibiotics. I. Taxonomy, production, isolation, characterization and properties. *J. Antibiot.* **33**, 364–376.
- Anzai, Y., Saito, N., Tanaka, M., Kinoshita, K., Koyama, Y. & Kato, F. (2003). Organization of the biosynthetic gene cluster for the polyketide macrolide mycinamicin in *Micromonospora griseorubida*. *FEMS Microbiol. Lett.* **218**, 135–141.
- Anzai, Y., Ishii, Y., Yoda, Y., Kinoshita, K. & Kato, F. (2004). The targeted inactivation of polyketide synthase *mycAV* in the mycinamicin producer, *Micromonospora griseorubida*, and a complementation study. *FEMS Microbiol. Lett.* **238**, 315–320.
- Anzai, Y., Li, S., Chaulagain, M. R., Kinoshita, K., Kato, F., Montgomery, J. & Sherman, D. H. (2008). Functional analysis of MycCI and MycG, cytochrome P450 enzymes involved in biosynthesis of mycinamicin macrolide antibiotics. *Chem. Biol.* **15**, 950–959.
- Li, S., Anzai, Y., Kinoshita, K., Kato, F. & Sherman, D. H. (2009). Functional analysis of MycE and MycF, two O-methyltransferases involved in the biosynthesis of mycinamicin macrolide antibiotics. *ChemBioChem*, **10**, 1297–1301.
- Tsukada, S., Anzai, Y., Li, S., Kinoshita, K., Sherman, D. H. & Kato, F. (2010). Gene targeting for O-methyltransferase genes, *mycE* and *mycF*, on the chromosome of *Micromonospora griseorubida* producing mycinamicin with a disruption cassette containing the bacteriophage ϕ C31 *attB* attachment site. *FEMS Microbiol. Lett.* **304**, 148–156.
- Schubert, H. L., Blumenthal, R. M. & Cheng, X. (2003). Many paths to methyltransfer: a chronicle of convergence. *Trends Biochem. Sci.* **28**, 329–335.
- Martin, J. L. & McMillan, F. M. (2002). SAM (dependent) I AM: the S-adenosylmethionine-dependent methyltransferase fold. *Curr. Opin. Struct. Biol.* **12**, 783–793.
- Rutherford, K., Le Trong, I., Stenkamp, R. E. & Parson, W. W. (2008). Crystal structures of human 108V and 108M catechol O-methyltransferase. *J. Mol. Biol.* **380**, 120–130.
- Vidgren, J., Svensson, L. A. & Liljas, A. (1994). Crystal structure of catechol O-methyltransferase. *Nature*, **368**, 354–358.
- Holm, L. & Rosenstrom, P. (2010). Dali server: conservation mapping in 3D. *Nucleic Acids Res.* **38**, W545–W549.
- Dyer, D. H., Wessely, V., Forest, K. T. & Lan, Q. (2008). Three-dimensional structure/function analysis of SCP-2-like2 reveals differences among SCP-2 family members. *J. Lipid Res.* **49**, 644–653.
- Haapalainen, A. M., van Aalten, D. M., Merilainen, G., Jalonen, J. E., Pirila, P., Wierenga, R. K. *et al.* (2001). Crystal structure of the liganded SCP-2-like domain of human peroxisomal multifunctional enzyme type 2 at 1.75 Å resolution. *J. Mol. Biol.* **313**, 1127–1138.
- Altschul, S. F., Gish, W., Miller, W., Myers, E. W. & Lipman, D. J. (1990). Basic local alignment search tool. *J. Mol. Biol.* **215**, 403–410.
- Singh, S., McCoy, J. G., Zhang, C., Bingman, C. A., Phillips, G. N., Jr. & Thorson, J. S. (2008). Structure and mechanism of the rebeccamycin sugar 4'-O-methyltransferase RebM. *J. Biol. Chem.* **283**, 22628–22636.
- Gomez Garcia, I., Stevenson, C. E., Uson, I., Freil Meyers, C. L., Walsh, C. T. & Lawson, D. M. (2010). The crystal structure of the novobiocin biosynthetic enzyme NovP: the first representative structure for the TylF O-methyltransferase superfamily. *J. Mol. Biol.* **395**, 390–407.
- Louie, G. V., Bowman, M. E., Tu, Y., Mouradov, A., Spangenberg, G. & Noel, J. P. (2010). Structure-function analyses of a caffeic acid O-methyltransferase from perennial ryegrass reveal the molecular basis for substrate preference. *Plant Cell*, **22**, 4114–4127.
- Huang, Y., Ji, L., Huang, Q., Vassilyev, D. G., Chen, X. & Ma, J. B. (2009). Structural insights into mechanisms of the small RNA methyltransferase HEN1. *Nature*, **461**, 823–827.
- Couture, J. F., Hauk, G., Thompson, M. J., Blackburn, G. M. & Trievel, R. C. (2006). Catalytic roles for carbon-

- oxygen hydrogen bonding in SET domain lysine methyltransferases. *J. Biol. Chem.* **281**, 19280–19287.
22. Fouces, R., Mellado, E., Diez, B. & Barredo, J. L. (1999). The tylosin biosynthetic cluster from *Streptomyces fradiae*: genetic organization of the left region. *Microbiology*, **145**, 855–868.
23. Hahn, D. R., Gustafson, G., Waldron, C., Bullard, B., Jackson, J. D. & Mitchell, J. (2006). Butenyl-spinosyns, a natural example of genetic engineering of antibiotic biosynthetic genes. *J. Ind. Microbiol. Biotechnol.* **33**, 94–104.
24. Patallo, E. P., Blanco, G., Fischer, C., Brana, A. F., Rohr, J., Mendez, C. & Salas, J. A. (2001). Deoxysugar methylation during biosynthesis of the antitumor polyketide elloramycin by *Streptomyces olivaceus*. *J. Biol. Chem.* **276**, 18765–18774.
25. Rodriguez, L., Rodriguez, D., Olano, C., Brana, A. F., Mendez, C. & Salas, J. A. (2001). Functional analysis of OleY L-oleandrosyl 3-O-methyltransferase of the oleandomycin biosynthetic pathway in *Streptomyces antibioticus*. *J. Bacteriol.* **183**, 5358–5363.
26. Torkkell, S., Ylihonko, K., Hakala, J., Skurnik, M. & Mantsala, P. (1997). Characterization of *Streptomyces nogalater* genes encoding enzymes involved in glycosylation steps in nogalamycin biosynthesis. *Mol. Gen. Genet.* **256**, 203–209.
27. Waldron, C., Matsushiba, P., Rostek, P. R., Jr, Broughton, M. C., Turner, J., Madduri, K. *et al.* (2001). Cloning and analysis of the spinosad biosynthetic gene cluster of *Saccharopolyspora spinosa*. *Chem. Biol.* **8**, 487–499.
28. Ward, S. L., Hu, Z., Schirmer, A., Reid, R., Revell, W. P., Reeves, C. D. *et al.* (2004). Chalomycin biosynthesis gene cluster from *Streptomyces bikiniensis*: novel features of an unusual ketolide produced through expression of the *chm* polyketide synthase in *Streptomyces fradiae*. *Antimicrob. Agents Chemother.* **48**, 4703–4712.
29. Ylihonko, K., Tuikkanen, J., Jussila, S., Cong, L. & Mantsala, P. (1996). A gene cluster involved in nogalamycin biosynthesis from *Streptomyces nogalater*: sequence analysis and complementation of early-block mutations in the anthracycline pathway. *Mol. Gen. Genet.* **251**, 113–120.
30. Tsuji, E., Okazaki, K., Isaji, M. & Takeda, K. (2009). Crystal structures of the apo and holo form of rat catechol-O-methyltransferase. *J. Struct. Biol.* **165**, 133–139.
31. Ding, Y. & Sherman, D. H. (2010). The role of synthesis and biosynthetic logic. In *Comprehensive Natural Products II*, pp. 559–579, Elsevier, Oxford, UK.
32. Li, S., Chaulagain, M. R., Knauff, A. R., Podust, L. M., Montgomery, J. & Sherman, D. H. (2009). Selective oxidation of carbolide C–H bonds by an engineered macrolide P450 mono-oxygenase. *Proc. Natl Acad. Sci. USA*, **106**, 18463–18468.
33. Akey, D. L., Kittendorf, J. D., Giraldez, J. W., Fecik, R. A., Sherman, D. H. & Smith, J. L. (2006). Structural basis for macrolactonization by the pikromycin thioesterase. *Nat. Chem. Biol.* **2**, 537–542.
34. Bolam, D. N., Roberts, S., Proctor, M. R., Turkenburg, J. P., Dodson, E. J., Martinez-Fleites, C. *et al.* (2007). The crystal structure of two macrolide glycosyltransferases provides a blueprint for host cell antibiotic immunity. *Proc. Natl Acad. Sci. USA*, **104**, 5336–5341.
35. Sherman, D. H., Li, S., Yermalitskaya, L. V., Kim, Y., Smith, J. A., Waterman, M. R. & Podust, L. M. (2006). The structural basis for substrate anchoring, active site selectivity, and product formation by P450 PikC from *Streptomyces venezuelae*. *J. Biol. Chem.* **281**, 26289–26297.
36. Kells, P. M., Ouellet, H., Santos-Aberturas, J., Aparicio, J. F. & Podust, L. M. (2010). Structure of cytochrome P450 PimD suggests epoxidation of the polyene macrolide pimaricin occurs via a hydroperoxoferric intermediate. *Chem. Biol.* **17**, 841–851.
37. Xu, L. H., Fushinobu, S., Takamatsu, S., Wakagi, T., Ikeda, H. & Shoun, H. (2010). Regio- and stereospecificity of filipin hydroxylation sites revealed by crystal structures of cytochrome P450 105P1 and 105D6 from *Streptomyces avermitilis*. *J. Biol. Chem.* **285**, 16844–16853.
38. Xue, Y. & Sherman, D. H. (2001). Biosynthesis and combinatorial biosynthesis of pikromycin-related macrolides in *Streptomyces venezuelae*. *Metab. Eng.* **3**, 15–26.
39. Xue, Y., Zhao, L., Liu, H. W. & Sherman, D. H. (1998). A gene cluster for macrolide antibiotic biosynthesis in *Streptomyces venezuelae*: architecture of metabolic diversity. *Proc. Natl Acad. Sci. USA*, **95**, 12111–12116.
40. Yang, M., Proctor, M. R., Bolam, D. N., Errey, J. C., Field, R. A., Gilbert, H. J. & Davis, B. G. (2005). Probing the breadth of macrolide glycosyltransferases: *in vitro* remodeling of a polyketide antibiotic creates active bacterial uptake and enhances potency. *J. Am. Chem. Soc.* **127**, 9336–9337.
41. Guerrero, S. A., Hecht, H. J., Hofmann, B., Biebl, H. & Singh, M. (2001). Production of selenomethionine-labelled proteins using simplified culture conditions and generally applicable host/vector systems. *Appl. Microbiol. Biotechnol.* **56**, 718–723.
42. Otwinowski, Z. & Minor, V. (1997). Processing of X-ray diffraction data collected in oscillation mode. *Macromolecular Crystallography, part A*, 276, pp. 307–326 Academic Press, New York, NY.
43. McCoy, A. J., Grosse-Kunstleve, R. W., Adams, P. D., Winn, M. D., Storoni, L. C. & Read, R. J. (2007). Phaser crystallographic software. *J. Appl. Crystallogr.* **40**, 658–674.
44. Adams, P. D., Afonine, P. V., Bunkoczi, G., Chen, V. B., Davis, I. W., Echols, N. *et al.* (2010). PHENIX: a comprehensive Python-based system for macromolecular structure solution. *Acta Crystallogr., Sect. D: Biol. Crystallogr.* **66**, 213–221.
45. Terwilliger, T. C. (2000). Maximum-likelihood density modification. *Acta Crystallogr., Sect. D: Biol. Crystallogr.* **56**, 965–972.
46. Terwilliger, T. C. (2003). Automated main-chain model building by template matching and iterative fragment extension. *Acta Crystallogr., Sect. D: Biol. Crystallogr.* **59**, 38–44.
47. Emsley, P. & Cowtan, K. (2004). Coot: model-building tools for molecular graphics. *Acta Crystallogr., Sect. D: Biol. Crystallogr.* **60**, 2126–2132.
48. Winn, M. D., Isupov, M. N. & Murshudov, G. N. (2001). Use of TLS parameters to model anisotropic displacements in macromolecular refinement. *Acta Crystallogr., Sect. D: Biol. Crystallogr.* **57**, 122–133.

49. Winn, M. D., Murshudov, G. N. & Papiz, M. Z. (2003). Macromolecular TLS refinement in REFMAC at moderate resolutions. *Methods Enzymol.* **374**, 300–321.
50. Painter, J. & Merritt, E. A. (2006). Optimal description of a protein structure in terms of multiple groups undergoing TLS motion. *Acta Crystallogr., Sect. D: Biol. Crystallogr.* **62**, 439–450.
51. Chen, V. B., Arendall, W. B., III, Headd, J. J., Keedy, D. A., Immormino, R. M., Kapral, G. J. *et al.* (2010). MolProbity: all-atom structure validation for macromolecular crystallography. *Acta Crystallogr., Sect. D: Biol. Crystallogr.* **66**, 12–21.
52. Davis, I. W., Leaver-Fay, A., Chen, V. B., Block, J. N., Kapral, G. J., Wang, X. *et al.* (2007). MolProbity: all-atom contacts and structure validation for proteins and nucleic acids. *Nucleic Acids Res.* **35**, W375–W383.
53. Chenna, R., Sugawara, H., Koike, T., Lopez, R., Gibson, T. J., Higgins, D. G. & Thompson, J. D. (2003). Multiple sequence alignment with the Clustal series of programs. *Nucleic Acids Res.* **31**, 3497–3500.
54. Thompson, J. D., Higgins, D. G. & Gibson, T. J. (1994). CLUSTAL W: improving the sensitivity of progressive multiple sequence alignment through sequence weighting, position-specific gap penalties and weight matrix choice. *Nucleic Acids Res.* **22**, 4673–4680.
55. Waterhouse, A. M., Procter, J. B., Martin, D. M., Clamp, M. & Barton, G. J. (2009). Jalview Version 2—a multiple sequence alignment editor and analysis workbench. *Bioinformatics*, **25**, 1189–1191.
56. The PyMOL Molecular Graphics System, Version 1.3, Schrödinger, LLC. <http://www.pymol.org>.